Biosensors and Bioelectronics 123 (2019) 204–210

Contents lists available at ScienceDirect

Biosensors and Bioelectronics

journal homepage: www.elsevier.com/locate/bios

Multiplex measurement of twelve tumor markers using a GMR multi-biomarker immunoassay biosensor

Yang Gao[a,b], Weisong Huo[a,b], Lei Zhang[c], Jie Lian[d], Wei Tao[c], Chuan Song[c], Jinping Tang[c], Stone Shi[c], Yunhua Gao[a,b,*]

[a] Key Laboratory of Photochemical Conversion and Optoelectronic Materials, Technical Institute of Physics and Chemistry, Chinese Academy of Sciences, Beijing 100190, China
[b] University of Chinese Academy of Sciences, Beijing 100049, China
[c] Dongguan Bosh Biotechnologies, LTD, Guangdong 523808, China
[d] Department of Forensic Science, People's Public Security University of China, Beijing 100038, China

ARTICLE INFO

Keywords:
GMR sensor chip
Microfluidic device
Magnetic nano-beads labelling
Twelve tumor markers
Multiplex measurement

ABSTRACT

Tumor markers play an important role in the early diagnosis and therapeutic effect monitoring of tumors. Combined detection of multiple tumor markers is a realistic way of improving the sensitivity and specificity of cancer diagnosis. To achieve this, we studied and designed a giant magneto resistance (GMR) multi-biomarker immunoassay biosensor that can simultaneously detect twelve kinds of tumor markers by integrating a GMR sensor chip, a microfluidic device, a magnetic nano-beads label, and a double antibody sandwich immunoassay method. As a proof of concept, the proposed immunosensor was utilized to detect 12 tumor markers (AFP, CEA, CYFRA21-1, NSE, SCC, PG I, PG II, CA19-9, total PSA, free PSA, free-β-hCG, Tg) and to screen patients with lung cancer, liver cancer, digestive tract cancer, prostatic cancer, etc. The immunosensor showed excellent sensitivity, accuracy, precision and stability. Designed as a POCT device, the immunosensor also allows for portability, able to perform rapid detection wherever necessary. As a multi-analyte assay, it provides significant advantages over single-analyte tests in terms of cost per test, labor and convenience. The system's ability to simultaneously measure the concentration of multiple markers in serum samples with excellent sensitivity and accuracy allows the immunosensor to be used for early tumor diagnosis.

1. Introduction

Precise measurement of tumor markers is vital in the early diagnosis and therapeutic effect monitoring of tumors (Brazhnik et al., 2015; Wang et al., 2012; Zhao et al., 2009). Currently, there exists many well-developed immunosensors for single tumor marker detection. However, due to the low specificity nature of tumor markers, a single tumor marker is usually not sufficient for cancer diagnosis; and the detection of a panel of tumor markers can significantly improve diagnostic value (Kulpa et al., 2002; Lenhard et al., 2011; Wang et al., 2017). Thus, multi-biomarker immunoassays have attracted increasing attention. In addition, multi-biomarker immunoassay possesses significant advantages over single-biomarker immunoassay in terms of cost, assay time, sample consumption, labor, and convenience (Wilson and Nie, 2006; Zong et al., 2012).

Multi-biomarker immunoassays primarily include two modes: multi-label and spatial resolution. (Wang and Ma, 2018; Wang et al., 2015; Zong et al., 2012). The Multi-label mode utilizes various labels, such as fluorescent materials (Tian et al., 2012; Wu et al., 2016) and metal compounds (Babamiri et al., 2018; Guo et al., 2013; Wang et al., 2018), to tag the antibodies or antigens of the corresponding analytes; as a result, it often suffers from a limited number of labels, signal overlapping, and differing optimal reaction conditions of these labels (Ge et al., 2013; Zhang et al., 2013). The spatial resolution mode employs spatial reaction location to distinguish different analytes on one substrate, and includes two modes: single-label and label-free. Label-free technologies such as surface plasmon resonance (McGrath et al., 2013) has emerged in recent years. However, because of their limited specificity, sensitivity and selectivity (Singh, 2016), the label-free mode has not been widely employed in clinical diagnosis. The single-label spatial-resolution mode uses one label to detect all analytes, and many research works in this field have been reported in recent years, such as

* Corresponding author at: Key Laboratory of Photochemical Conversion and Optoelectronic Materials, Technical Institute of Physics and Chemistry, Chinese Academy of Sciences, Beijing 100190, China.
E-mail address: yhgao@mail.ipc.ac.cn (Y. Gao).

https://doi.org/10.1016/j.bios.2018.08.060
Received 28 June 2018; Received in revised form 22 August 2018; Accepted 25 August 2018
Available online 25 August 2018
0956-5663/

fluorescence (Ge et al., 2013), chemiluminescence (Zong et al., 2012), electrochemiluminescence (Zhang et al., 2013), electrochemical (Wilson and Nie, 2006), magnetic (Wang et al., 2015), and surface enhanced Raman scattering (Zhang et al., 2018). Among these technologies, a spatial resolution multi-biomarker immunoassay method utilizing a giant magneto resistance (GMR) chip and magnetic nano-beads label has attracted many researchers (Manteca et al., 2011; Rife et al., 2003; Wang et al., 2015). The GMR sensor's signal is emitted from the magnetic excitation of the magnetic labels on the sensor's surface, and every sensor is able to work independently and monitored simultaneously. The advantages of GMR immunoassay technology include low costs, high portability, excellent sensitivity, low background noise, and real-time signal readout. Moreover, because of its ease of integration and miniaturization, GMR immunoassay technology has the potential to be employed in a multi-biomarker point-of-care test (POCT) diagnostic device (Choi et al., 2016).

The advantages of microfluidics technology include low consumption of reagents, a rapid reaction rate, high reaction efficiency, automation, and being environmentally friendly (Busin et al., 2016; Jung et al., 2015; Su et al., 2015). Furthermore, this technology is excellent in terms of compatibility with GMR sensors. Thus, the combination of the GMR immunoassay technology and microfluidics technology yields a very competitive POCT platform. We studied and designed a GMR multi-biomarker POCT diagnostic system capable of simultaneously detecting twelve different tumor markers by integrating a GMR sensor chip, a microfluidic magnetic nano-beads label, and a double antibody sandwich immunization method. The biomarkers studied are alpha-fetoprotein (AFP, 70 kDa), carcinoembryonic antigen (CEA, 180 kDa), cytokeratin 19 fragment (CYFRA21-1, 40 kDa), neuron specific enolase (NSE, 47 kDa), free β-subunit of human chorionic gonadotropin (free-β-hCG, 23.5 kDa), squamous cell carcinoma (SCC, 45 kDa), pepsinogen I (PG I, 42 kDa), pepsinogen II (PG II, 42 kDa), total prostate specific antigen (total PSA, tPSA, including PSA-ACT (90 kDa) and free PSA), free prostate specific antigen (free PSA, fPSA, 34 kDa), thyroglobulin (Tg, 660 kDa), and carbohydrate antigen 19-9 (CA19-9, > 400 kDa) (Björk et al., 1998; Czinn and Blanchard, 2011; Lund et al., 2014; Marrakchi et al., 2008; Nustad et al., 2004; Paus et al., 2011; Wilson and Nie, 2006).

2. Materials and methods

2.1. Antibodies and antigens

Anti-human AFP antibodies (clones 19B12, 0105E11, 14D9) and anti-human PG I antibodies (clones 1.9A02 and 2.3E11) were purchased from Cholun Medicine, LTD. (China), anti-human CEA antibodies (clones 1C1, 3E1 and 3E3) and anti-human CYFRA21-1 antibodies (clones 2F3 and 1A6) were purchased from Fapon Biology, LTD. (China), anti-human NSE antibodies (clones 9601 and 9602) and anti-human Tg antibodies (clones 2802, 2803 and 2805) were purchased from Medix Biochemica (Finland), anti-human free-β-hCG antibodies (catalog No: M050401, M050402 and M050403) were purchased from Biogenome Biotechnologies, LTD. (China), anti-human SCC antibodies (catalog No: H083001 and H083002) were purchased from Orinia Biotechnologies, LTD. (China), anti-human CA19-9 antibodies (clones M2012114 and M2012113) were purchased from Fitzgerald Industries International, Inc. (USA), anti-human PG II antibodies (catalog No: A45290 and A45300) were purchased from Biospacific, Inc. (USA), anti-human total PSA capture antibodies (clones 8311 and 8312) were purchased from Medix Biochemica, anti-human free PSA capture antibody (catalog No: A45501) were purchased from Biospacific, Inc, anti-human total PSA and free PSA detection antibodies (catalog No: M165) were purchased from Calbioreagents, Inc. (USA), AFP, CEA, NSE, PG I, total PSA, free PSA, Tg, and CA19-9 antigens were purchased from Fitzgerald Industries International, Inc., PG II and free-β-hCG antigens were purchased from Biospacific, Inc., CYFRA21-1 antigens were purchased from Calbioreagents, Inc., SCC antigens were purchased from Fujirebio Diagnostics, Inc. (Sweden), N-hydroxysuccinimidobiotin (NHS-Biotin), succinimidyl-6-(biotinamido) hexanoate (NHS-LC-Biotin), succinimidyl-6-(biotinamido)-6-hexanamidohexanoate (NHS-LC-LC-Biotin), Hydrazide-LC-Biotin and Maleimide-PEG_2-Biotin were purchased from Thermo Fisher Scientific, Inc. (USA), streptavidin conjugated superparamagnetic particles were purchased from Ademtech (French), and clinical serum samples were from Zhujiang Hospital of Southern Medical University (China).

2.2. Buffers

Carbonate buffer (CB, 0.1 M, pH 9.6), consisting of Na_2CO_3 and $NaHCO_3$, was used for the immobilization of the capture antibody. CBT (pH 9.6), used to prepare and re-dissolve the streptavidin magnetic particles solution, was 0.1 M CB spiked with 0.05% Tween-20. Phosphate-buffered saline (PBS; 0.01 M, pH 7.4), created by mixing NaH_2PO_4 and Na_2HPO_4. PBST (pH 7.4), used to prepare the labelling antibodies solution, was 0.01 M PBS spiked with 0.05% Tween-20. Washing buffer was 0.01 M PBS spiked with 0.1% Tween-20.

2.3. Apparatus

The GMR immunoassay analyser is manufactured by Bosh Biotechnologies, LTD. (China), the Nano-plotter (NP 2.1) is manufactured by GeSim. (Germany), the spin coater is manufactured by the institute of microelectronics of chinese academy of sciences (China), the ultraviolet radiation lamp (254 nm) is manufactured by the technical institute of physics and chemistry of chinese academy of sciences (China), the refrigerated centrifuge is manufactured by Sigma (Germany), the EASY pure LF ultrapure water system is manufactured by Barnstead (USA).

2.4. Fabrication of test card

As illustrated in Fig. 1b, the test card (Fig. 1a) mainly consists of six layers: the top cover, the polydimethylsiloxane (PDMS) lid, the reagent reservoir layer, the PDMS thin layer, the Printed Circuit Board (PCB) with the GMR chip (Fig. 1c), and the bottom cover. The reagent reservoir layer, made of ABS, contains a sample cavity, a washing solution cavity, and a magnetic nano-beads solution cavity. The PDMS lid is fixed at the top of the reagent reservoir layer and used to seal the reagent reservoir cavities. The microfluidic channel, fabricated at the bottom of the reagent reservoir layer, connects the reagent reservoir to the reaction chamber over the chip. The PDMS thin film is used for sealing the microfluidic channel. The microfluidic control system employed pressure-driven flow mode. The PDMS lid is elastic, so when under pressure from the stepping motor, the reagents in the reservoir cavity could be pushed into the reaction zone to participate in the immune reaction processes. Furthermore, the pumping mechanism on the reagent reservoir cavity could drive the fluid in both directions, allowing for a back-and-forth motion of the fluid under a controlled speed and distance, significantly improving the efficiency and speed of the biochemical reaction process.

2.5. GMR chip fabrication and surface functionalization

The GMR multilayer structure consists of a stacked structure of thin films of Si (450 μm) /SiO_2 (10 nm)/ Ta (4.5 nm)/ PtMn (10 nm)/ CoFe (2 nm)/ Cu (1.2 nm)/ CoFe (1 nm)/ NiFe (3 nm)/ Al_2O_3 (40 nm). As shown in Fig. 1c, the GMR chip contained 40 individual GMR sensors (with a diameter of 120 μm). Each sensor could detect one kind of protein, so the proposed immunosensor could simultaneously detect 40 different proteins. Alternatively, a protein could be detected using two or more capture antibodies, one with a strong reactivity and one with a weak one (Figs. 5a- 5e), improving both detection sensitivity and linear

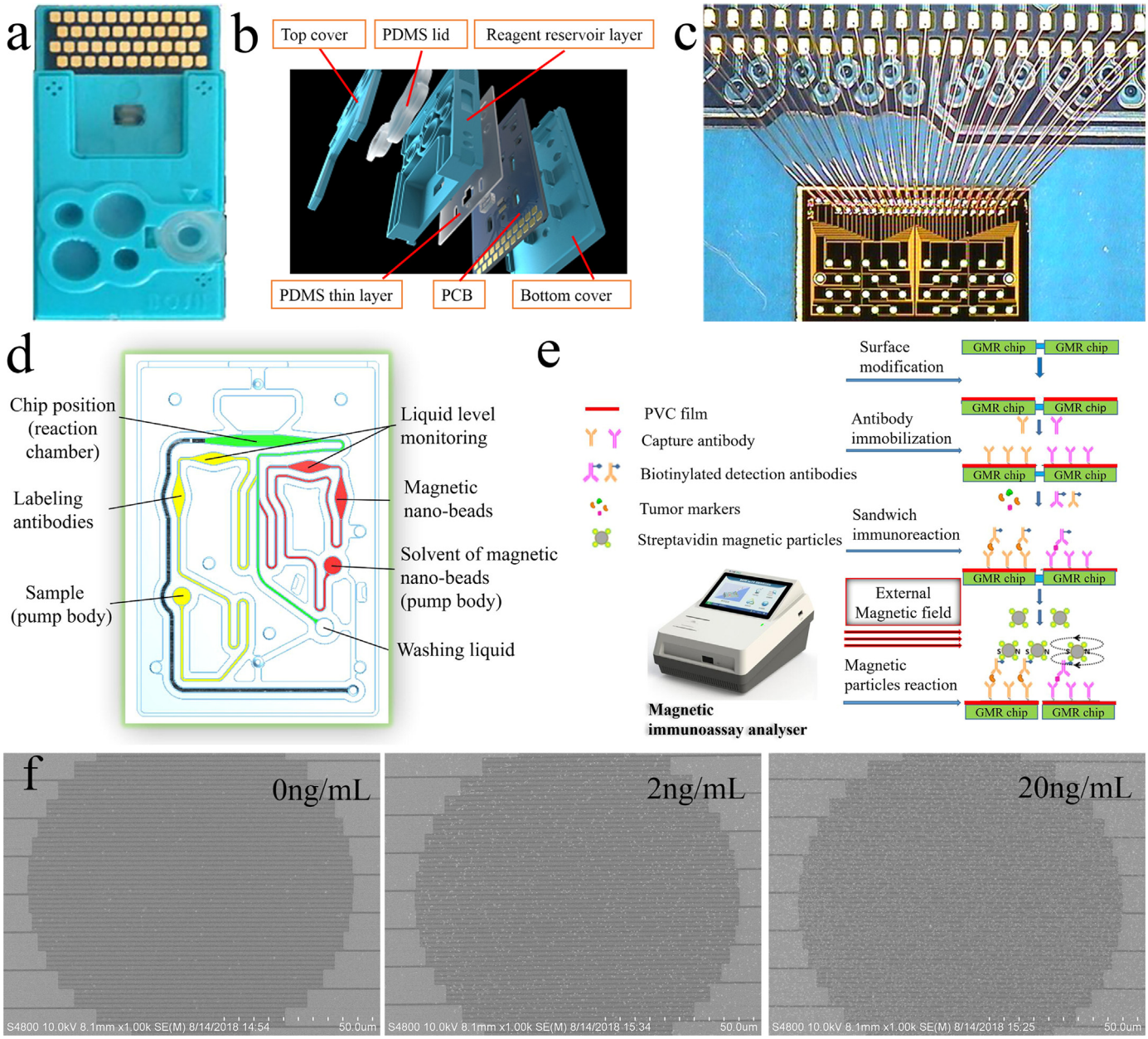

Fig. 1. (a) The test card, (b) The multilayer structure of the test card, (c) GMR chip and the connection between the GMR chip and PCB, (d) The structure of the microchannel system, (e) The reaction process of the GMR multi-biomarker immunoassay. (f) SEM images of magnetic nano-beads bound on GMR sensor surface after protein assay. The three images are for CEA assay with different concentrations.

dynamic range.

Because the adsorption ability of proteins on the GMR chip surface was weak, modification of the GMR chip surface was necessary. First, the GMR chip surface was modified with polyvinyl chloride (PVC) via spin coating technique, and then transferred into a high temperature oven to be baked at 70 °C for 10 min. Capture antibodies are spotted on the surface of the GMR sensor by a nano-plotter. Before the plotting process, in order to improve the adsorption efficiency of capture antibodies, the GMR chips are treated for 10 min via ultraviolet ozone radiation method.

2.6. Microchannel system and immunoassay procedure

The micro-channel system consists primarily of three components (Fig. 1d): a sample channel, a washing solution channel, and a magnetic nano-beads solution channel. A nano-plotter spotted different kinds of capture antibodies on individual GMR sensors. 5 μL biotinylated labelling antibodies and 4 μL magnetic nano-beads were lyophilized and stored in the corresponding position of the micro-channel, and the whole reaction process was controlled to take place at 37 °C. The reaction step is shown in Fig. 1e. 50 μL sample solution was first added to sample cavity, and then the sample solution was injected into the sample level monitoring position. The up and down pressing of the PDMS film on the sample cavity made the sample solution oscillate back and forth in the sample micro-channel, ensuring the labelling antibodies to dissolve thoroughly. Second, a mixture of analytes and labelling antibodies were pumped onto the GMR sensor surface and then captured through immuno-reaction. The back-and-forth motion of the mixture solution in the reaction chamber significantly improved the efficiency and speed of the biochemical reaction process. Third, cleaning solution was injected to wash away the remaining analytes and labelling antibodies. Finally, the CBT solution was injected into the

magnetic nano-beads liquid position monitoring location, and after the streptavidin magnetic nano-beads were dissolved thoroughly in CBT solution, the magnetic nano-beads solution was pumped into the reaction chamber and captured by the biotinylated labelling antibodies. As shown in Fig. 1f, the higher the concentration of the analyte, the more magnetic nano-beads would be coupled on the GMR sensor. The magnetic nano-beads attached to the GMR sensor generate a stray magnetic field in the presence of an alternating current (AC) magnetic field, and the stray magnetic field reduces the AC magnetic field. The change of the AC magnetic field results in a change in the resistance of the GMR sensor, which is measured and mapped into the domain of analyte concentration. Using this design, the system can simultaneously measure the concentrations of 12 different tumor markers.

2.7. GMR immunoassay analyser

The GMR immunoassay analyser mainly consists of four parts: the temperature control system, the microfluidic actuating system, the signal processing system, and the data processing system. The temperature control system employed an infrared temperature sensor to ensure the immunoreaction was running at 37 °C. The microfluidic actuating system was controlled by stepping motors. One millimeter driving distance of the stepping motor was divided into 25,000 steps, or in other words, the driving distance of each step was 40 nm. As shown in Fig. 1d, the diameter of the pump body of the micro-channel was about 3 mm; in terms of volume, each step of the stepping motor actuate 2.8 nL reagent.

The signal processing system consists of two modules: electrical and magnetic. Specifically, in the presence of an AC magnetic field, magnetic nano-beads attached on the surface of the chip introduce a stray magnetic field and induce a change in the GMR sensors' resistance. The sensor's output signal is connected to a transimpedance amplifier. Finally, an analogue to digital converter (DAC) converts the amplifier's signals to digital values. The data processing system transforms the DAC's signals to concentration values based on their respective calibration curves. The measurement results can be transmitted via a WIFI network, and can be uploaded to a doctor's data base immediately.

3. Results and discussion

3.1. Antibody immobilization

The capture antibodies are attached to the surface of the PVC membrane by hydrophobic interaction. However, because of the strong hydrophobicity of PVC, the capture antibodies' solution was difficult to spread across the surface of the PVC membrane. The hydrophobicity of the PVC membrane can be optimized through ultraviolet ozone radiation method. The ultraviolet radiation time can significantly affect the properties of PVC membrane, so the radiation time was optimized using 100 ng/mL AFP, CEA, PG I and PG II at a wavelength of 254 nm. The results showed that the optimum time for ultraviolet radiation was 10 min (Fig. 2a). The capture antibodies' concentration was another important factor. The capture antibodies acted as surfactants in the capture antibodies solution. As shown in Fig. 2b, when the capture antibodies' concentration was relatively low, the capture antibody solution was difficult to spread across the surface of the PVC membrane. Increasing the capture antibodies' concentration led to an increase in the coverage area of the capture antibodies and the reaction signals (rate of resistance changes) of AFP, CEA, PG I, and PG II, and all the signals reached a constant value when the capture antibodies solution was beyond 50 μg/mL (Fig. 2c). Thus, 50 μg/mL was selected as the optimal capture antibodies' concentration.

3.2. Magnetic nano-beads label

The magnetic nano-beads label is a significant factor in the GMR immunosensor's detection performance which is characterized by the immunosensor's response signal, background noise, and dynamic range. The 128 nm magnetic nano-beads were the best choice for the proposed immunosensor (Huo et al., 2015). The concentration of the magnetic nano-beads is another important factor affecting the immunosensor's performance. Fig. S1 in Supporting information shows that increasing the magnetic nano-beads' concentration increased the reaction signals of PSA and CEA until 75 mg/mL, while the background noise was largely unchanged. Therefore, the optimal choice of the magnetic beads for the immunosensor is 75 mg/mL with a diameter of 128 nm.

3.3. Biotinlated antibodies

A biotin-avidin system can significantly enhance the conjugating effect between the magnetic nano-beads and the labelling antibodies. Because the biotin group is relatively small, biotin can be conjugated to many antibodies without altering their biological activities. The proposed immunosensor employs the biotin-avidin amplification system, and we analysed the influence of the biotin compounds containing different reactive groups or spacer arm lengths on the analytical sensitivity and linear range of the proposed immunosensor. Specifically, NHS-Biotin (Space arm length: 13.5 Å), NHS-LC-Biotin (Space arm length: 22.4 Å), and NHS-LC-LC-Biotin (Space arm length: 30.5 Å) conjugated with the primary amino groups (-NH_2) of antibodies to form stable amide bonds. Maleimide-PEG_2-Biotin (Space arm length: 29.1 Å) reacted efficiently with reduced sulfhydryl groups (-SH) to form stable thioether bonds. Hydrazide-LC-Biotin (Space arm length: 24.7 Å) reacted with carbonyl groups, created by oxidation reaction of carbohydrate groups, to form stable hydrazone bonds.

Because the binding sites on avidin for biotin is somewhat buried below the surface of the antibodies, some biotin molecules may not conjugate with avidin effectively. A long-chain biotin compound can result in better binding potential for avidin. For AFP, CYFRA21-1, PG II, Tg, free-β-hCG, PSA, and fPSA (Fig. 3. a-e and g-h), NHS-LC-Biotin and

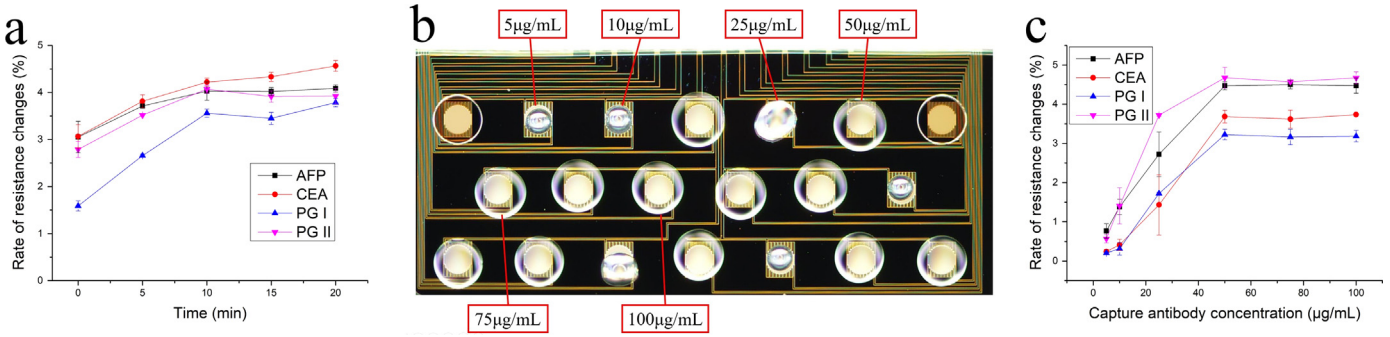

Fig. 2. (a) The impact of ultraviolet radiation time on reactivity, (b) The impact of capture antibodies concentration on the morphology of spotting after drying, (c) The impact of capture antibodies concentration on reactivity.

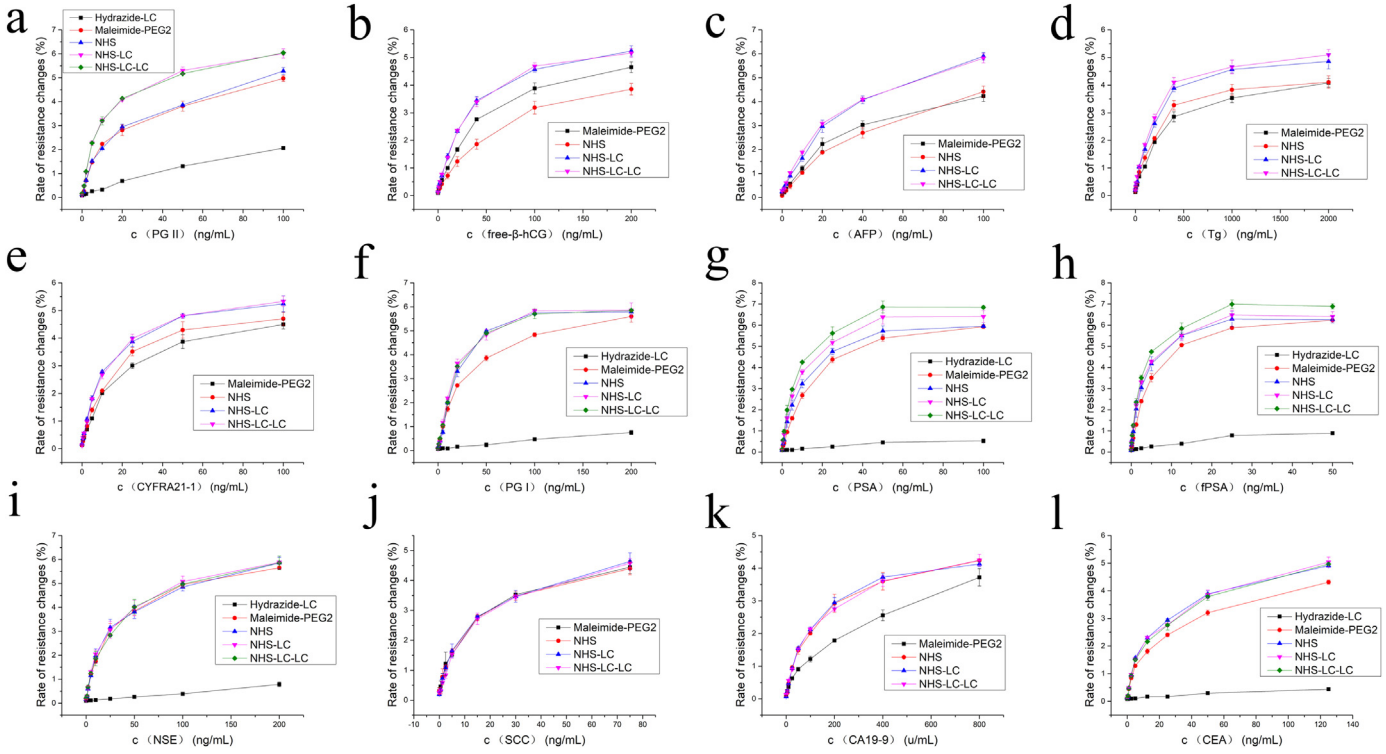

Fig. 3. The impact of different biotin compounds on the reactivity of the proposed immunosensor.

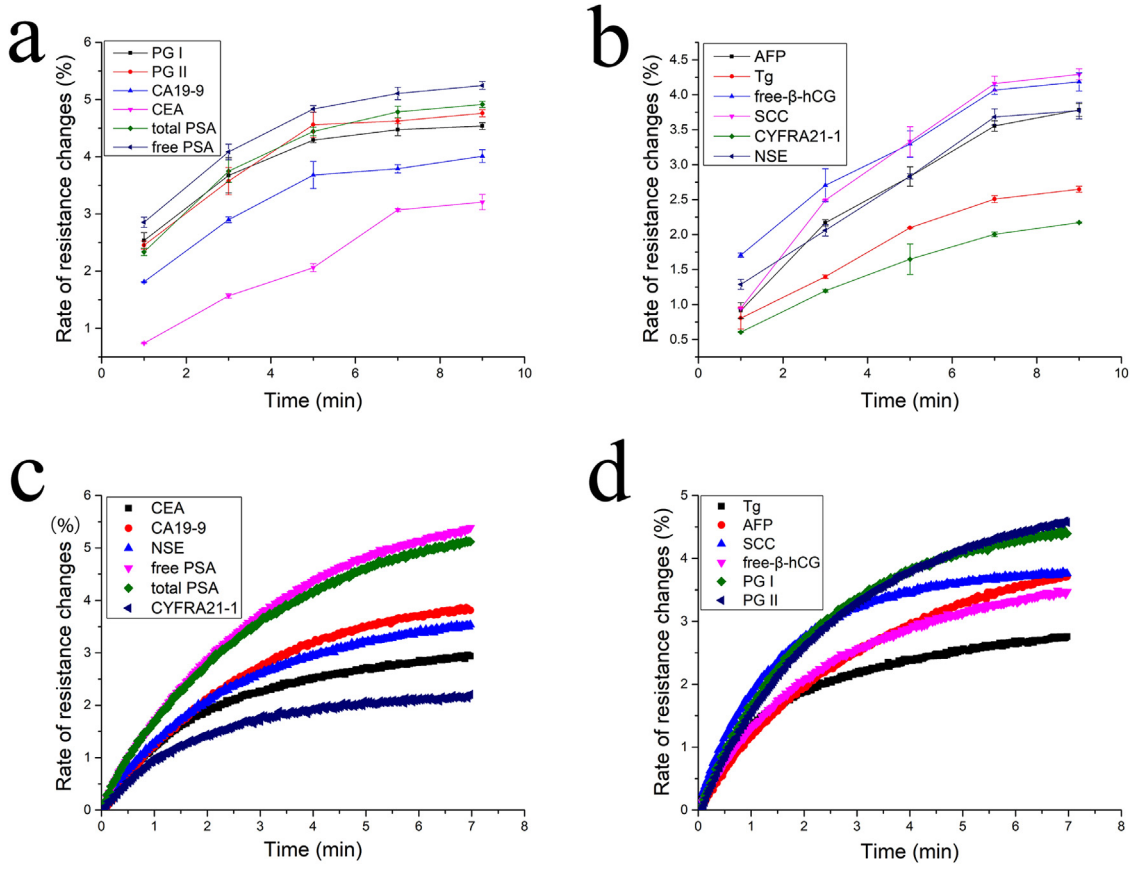

Fig. 4. The effect of the incubation time. (a) and (b): sandwich immunoreaction, (c) and (d): magnetic nano-beads labelling reaction.

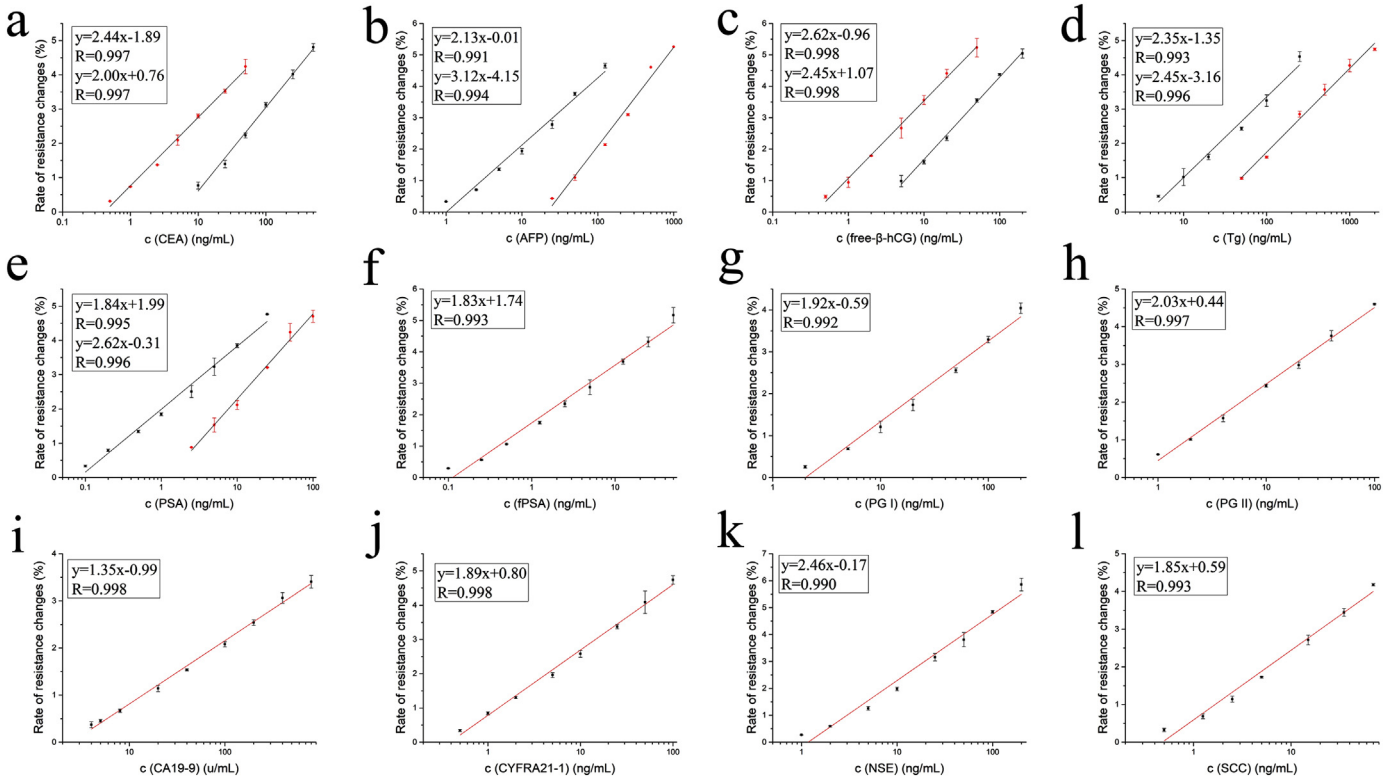

Fig. 5. Calibration curves for the 12 tumor markers immunoassay. (a)- (e): using two capture antibodies to measure the tumor markers, (f)-(l) using one capture antibody to measure the tumor marker.

NHS-LC-LC-Biotin showed better reactivity than NHS-Biotin. By contrast, the binding sites on some antibodies are not buried inside the surface plane, so the increased spacer arm length may not significantly change the conjugating effect between magnetic nano-beads and labelling antibodies. For example, CEA, NSE, PG I, CA19-9 and SCC (Fig. 3. f and i-l), the reactivity of NHS-LC biotin and NHS-LC-LC biotin labelling was essentially the same as NHS-biotin labelling. The reactive group is another important factor for the biotin-avidin system, and the results showed that the order of reactivity of different reactive groups was as follows (sequentially from high to low): amine-reactive biotin, sulfhydryl-reactive biotin, and carbonyl-reactive biotin.

For the proposed immunosensor, the reactivity of Hydrazide-LC-Biotin was too weak to meet the detection requirements (Fig. 3. a, f-i and l). NHS-LC-Biotin or NHS-LC-LC-Biotin labelling could significantly improve reactivity and did not affect high concentration detection, and was applied to label Tg, PG II, CYFRA21-1, AFP, and free-β-hCG antibodies (Fig. 3. a-e). Although the reactivity of Maleimide-PEG_2-Biotin was slightly lower than amine-reactive biotins, it offered a large dynamic range for high concentration test. Consequently, maleimide-PEG_2-Biotin was favored for high concentration detection, and was applied to PG I, PSA and fPSA (Fig. 3. f-h). Since the reaction behavior of CEA, NSE, CA19-9, and SCC were similar, and since NHS-Biotin labelling method was the simplest and cheapest, NHS-Biotin labelling was chosen for CEA, NSE, CA19-9, and SCC (Fig. 3.i-l).

3.4. Optimization of incubation time

An important design objective of the GMR multi-biomarker immunoassay biosensor is to provide prompt diagnostic results for point-of-care diagnostics and treatment. To ensure the immunosensor's performance in the simultaneous detection of the 12 tumor makers, the incubation time of the sandwich immunoreaction and the incubation time of the magnetic nano-beads labelling were evaluated using a total of 100 ng/mL of PSA, CEA, and PG II, 50 ng/mL of free PSA, AFP, and NSE, 10 ng/mL of CYFRA21-1, 80 ng/mL of free-β-hCG, 25 ng/mL of SCC, 200 ng/mL of PG I, 250 ng/mL of Tg, and 400 u/mL of CA19-9. As shown in Fig. 4, the signals of the 12 tumor markers increased as the incubation time prolonged, and the preferred incubation time of the sandwich immunoreaction and the magnetic nano-beads were 7 min and 6 min, respectively, and it is approximately the same for all 12 tumor markers. Moreover, there was no noticeable increase in background noise as incubation time increased. As a result, the proposed immunosensor could finish detecting all 12 tumor markers in 15 min with cleaning time included.

3.5. Assay performance

The calibration curve was determined by measuring various concentrations of tumor marker antigens. As shown in Fig. 5, the immunosensor's reaction signals had a linear response with the logarithm of analyte concentrations in the range of 0.5–500 ng/mL for CEA, 1–1000 ng/mL for AFP, 0.1–100 ng/mL for total PSA, 0.1–50 ng/mL for free PSA, 2–200 ng/mL for PG I, 1–100 ng/mL for PG II, 0.5–100 ng/mL for CYFRA21-1, 1–200 ng/mL for NSE, 0.5–200 ng/mL for free-β-hCG, 0.5–70 ng/mL for SCC, 5–2000 ng/mL for Tg, and 4–800 U/mL for CA19-9. The analytical sensitivity (the limits of detection) was defined as the concentration at three standard deviations above the mean value of background (0 ng/mL). The calculated analytical sensitivity is shown in Table 1. The proposed immunosensor exhibited high analytical sensitivity and a relatively broad linear range.

Stability and precision are two other key performance indices for evaluating a successful immunosensor. The proposed immunosensor was designed to have an imprecision of less than 10% coefficient of variation (CV). The test imprecision of the 12 tumor markers was evaluated by measuring two different concentrations of quality control reagents using their respective calibration curves. As shown in Table 1, with the exception of a low concentration of SCC, the proposed immunosensor showed good precision and met the design requirements,

Table 1
The analytical sensitivity and intra-assay precision of the proposed immunosenor.

Analyte	analytical sensitivity [c]	Intra-assay imprecision [d]		Intra-assay imprecision [d]	
		Mean	CV, %	Mean	CV, %
AFP [a]	0.52	25	7.6	183.9	8.9
CEA [a]	0.27	6	6.7	101.7	5.7
CYFRA21-1 [a]	0.25	3.3	8.4	47	7.6
NSE [a]	0.5	18.2	7.1	69.2	7.5
SCC [a]	0.3	2.3	13.7	30.3	7.8
PGI[a]	1	34.4	9.6	82.4	9.1
PGII[a]	0.5	14.1	3.5	40.9	5.8
CA19-9 [b]	2	31.6	8.8	163.7	6.8
total PSA [a]	0.02	2.2	6.7	34.5	9.5
free PSA [a]	0.07	1	7.6	9.1	9.3
free-β-hCG [a]	0.3	5.9	7.2	98.5	6.0
Tg [a]	1	67.9	6.9	461.1	5.3

[a] ng/mL, [b] u/mL, [c] The proposed immunosensor's analytical sensitivity and intra-assay imprecision in testing the twelve tumor markers.

with intra-assay CVs being less than 10%. The precision of the high concentration SCC was excellent. However, nonspecific adsorption caused a strong background interference, which affected the precision of the detection of low concentration SCC. The intra-assay CV of low concentration SCC was 13.7%, even though it meets the clinical requirements (intra-assay CV was less than 15%). The stability of the test cards was evaluated in dry conditions at 37 °C. Shown in Fig. S2 of the supporting information, the detection concentrations of 12 tumor markers did not show significant change for 1 week, demonstrating good stability.

We also compared the performance of our proposed assay with that of commercially available single analyte assays and previously reported multi-analyte assays. The data in Table S1 (supplementary material) indicate that both the analytical sensitivity and the upper limit of detection of the proposed immunosenor either are comparable or exceed that of the commercial single-analyte immune assays. Compared with previously reported multi-biomarker detection methods (Table S2, supplementary material), the proposed immunosensor exhibits a wider linear range (Brazhnik et al., 2015; Wilson and Nie, 2006; Zhao et al., 2009) and offers simplified operation which requires no dilution process (Zhang et al., 2013; Zong et al., 2012), sample pre-treatment or protein purification (Tian et al., 2012).

3.6. Methodological comparison

In order to evaluate the reliability of the proposed immunosensor, it was compared to Architect (for SCC, PG I, PG II) and Roche (for CEA, AFP, total PSA, free PSA, CYFRA21-1, NSE, free-β-hCG, Tg, CA19-9). The comparison was carried out by measuring clinical samples. Fig. S3 in the supplementary material shows that, compared to commercial immunosensors, the proposed immunosensor had good correlation coefficients ($R^2 > 95\%$) and slopes (close to 1) for the detection of 12 tumor markers.

4. Conclusions

By integrating a GMR sensor chip, a microfluidic device, a magnetic nano-beads label, and utilizing the classical double antibody sandwich immunoassay method, we developed a novel GMR multi-biomarker immunoassay biosensor capable of simultaneously quantify 12 tumor markers in 15 min. The proposed immunosensor had a wide detection range, high sensitivity, excellent precision, clinically acceptable accuracy and good storage stability. As opposed to previously reported multi-biomarker detection methods, the proposed immunosensor offers a platform for real world clinical application with clinically acceptable performance. Compared with commercially available single analyte assays, the proposed multi-biomarker assay is advantageous in terms of cost, assay time, reagent consumption, labor, and convenience. A limitation of this technology is that its high sensitivity limits its use on biomarkers which requires a very high upper-limit-of-detection. We'll study alternative biomarkers which are compatible with this platform and meet the requirement of clinical applications. Additionally, we'll be studying new biomarkers which might bring improved diagnostic performance over the commonly used biomarkers. The correlative nature of the multiplex test results of this technology allows the possibility for comparative study to be carried out efficiently.

Acknowledgements

This research was financed by the 2014 Major Project Fund of Dongguan City, China (2014215102) and the Science and Technology Planning Project of Guangdong Province (2015B020233001).

Appendix A. Supporting information

Supplementary data associated with this article can be found in the online version at doi:10.1016/j.bios.2018.08.060.

References

Babamiri, B., Hallaj, R., Salimi, A., 2018. Biosens. Bioelectron. 99, 353–360.
Björk, T., Ljungberg, B., Piironen, T., Abrahamsson, P.-A., Pettersson, K., Cockett, A.T.K., Lilja, H., 1998. Urology 51, 57–62.
Brazhnik, K., Sokolova, Z., Baryshnikova, M., Bilan, R., Efimov, A., Nabiev, I., Sukhanova, A., 2015. Nanomed. Nanotechnol. 11, 1065–1075.
Busin, V., Wells, B., Kersaudy-Kerhoas, M., Shu, W., Burgess, S.T.G., 2016. Mol. Cell. Probe. 30, 331–341.
Choi, J., Gani, A.W., Bechstein, D.J.B., Lee, J.-R., Utz, P.J., Wang, S.X., 2016. Biosens. Bioelectron. 85, 1–7.
Czinn, S.J., Blanchard, S.S., 2011. Developmental Anatomy and Physiology of the Stomach. In: Wyllie, R., Hyams, J.S. (Eds.), Pediatric Gastrointestinal and Liver Disease, Fourth edition. W.B. Saunders, Saint Louis, pp. 262–268.
Ge, S., Ge, L., Yan, M., Song, X., Yu, J., Liu, S., 2013. Biosens. Bioelectron. 43, 425–431.
Guo, Z., Hao, T., Du, S., Chen, B., Wang, Z., Li, X., Wang, S., 2013. Biosens. Bioelectron. 44, 101–107.
Huo, W., Gao, Y., Zhang, L., Shi, S., 2015. IEEE Trans. Magn. 51, 1–4.
Jung, W., Han, J., Choi, J.-W., Ahn, C.H., 2015. Microelectron. Eng. 132, 46–57.
Kulpa, J., Wójcik, E., Reinfuss, M., Kołodziejski, L., 2002. Clin. Chem. 48, 1931.
Lenhard, M., Stieber, P., Hertlein, L., Kirschenhofer, A., Fürst, S., Mayr, D., Nagel, D., Hofmann, K., Krocker, K., Burges, A., 2011. Clin. Chem. Lab. Med. 49, 2081–2088.
Lund, H., Paus, E., Berger, P., Stenman, U.-H., Torcellini, T., Halvorsen, T.G., Reubsaet, L., 2014. Tumor Biol. 35, 1013–1022.
Manteca, A., Mujika, M., Arana, S., 2011. Biosens. Bioelectron. 26, 3705–3709.
Marrakchi, R., Ouerhani, S., Benammar, S., Rouissi, K., Bouhaha, R., Bougatef, K., Messai, Y., Khadimallah, I., Rahal, K., Ben Ammar-Elgaaied, A., 2008. Int. J. Biol. Marker 23, 238–243.
McGrath, T.F., Buijs, J., Huet, A.C., Delahaut, P., Elliott, C.T., Mooney, M.H., 2013. Sens. Actuators B 186, 423–430.
Nustad, K., Dowell, B.L., Davis, G.J., Stewart, K., Nilsson, O., Röijer, E., Suminami, Y., Nawata, S., Cataltepe, S., Silverman, G.A., Kato, H., de Bruijn, H.W.A., 2004. Tumor Biol. 25, 69–90.
Paus, E., Hirzel, K., Lidqvist, M., Höyhtyä, M., Warren, D.J., 2011. Tumor Biol. 32, 819–829.
Rife, J.C., Miller, M.M., Sheehan, P.E., Tamanaha, C.R., Tondra, M., Whitman, L.J., 2003. Sens. Actuators A 107, 209–218.
Singh, P., 2016. Sens. Actuators B 229, 110–130.
Su, W., Gao, X., Jiang, L., Qin, J., 2015. J. Chromatogr. A 1377, 13–26.
Tian, J., Zhou, L., Zhao, Y., Wang, Y., Peng, Y., Zhao, S., 2012. Talanta 92, 72–77.
Wang, H., Ma, Z., 2018. Sens. Actuators B 256, 402–407.
Wang, W., Xu, X., Tian, B., Wang, Y., Du, L., Sun, T., Shi, Y., Zhao, X., Jing, J., 2017. Clin. Chim. Acta 470, 51–55.
Wang, Y., Fang, F., Shi, C., Zhang, X., Liu, L., Li, J., Zhou, X., Yao, J., Kang, X., 2012. Clin. Biochem. 45, 1394–1398.
Wang, Y., Wang, W., Yu, L., Tu, L., Feng, Y., Klein, T., Wang, J.-P., 2015. Biosens. Bioelectron. 70, 61–68.
Wang, Z., Yang, H., Wang, M., Petti, L., Jiang, T., Jia, Z., Xie, S., Zhou, J., 2018. Colloid Surf. A 546, 48–58.
Wilson, M.S., Nie, W., 2006. Anal. Chem. 78, 6476–6483.
Wu, S., Liu, L., Li, G., Jing, F., Mao, H., Jin, Q., Zhai, W., Zhang, H., Zhao, J., Jia, C., 2016. Talanta 156–157, 48–54.
Zhang, D., Huang, L., Liu, B., Ni, H., Sun, L., Su, E., Chen, H., Gu, Z., Zhao, X., 2018. Biosens. Bioelectron. 106, 204–211.
Zhang, Y., Liu, W., Ge, S., Yan, M., Wang, S., Yu, J., Li, N., Song, X., 2013. Biosens. Bioelectron. 41, 684–690.
Zhao, Y., Zhao, X., Pei, X., Hu, J., Zhao, W., Chen, B., Gu, Z., 2009. Anal. Chim. Acta 633, 103–108.
Zong, C., Wu, J., Wang, C., Ju, H., Yan, F., 2012. Anal. Chem. 84, 2410–2415.